

Observing white dwarfs orbiting massive black holes in the gravitational wave and electro-magnetic window

A. Sesana¹, A. Vecchio², M. Eracleous^{1,3} and S. Sigurdsson^{1,3}

¹ Center for Gravitational Wave Physics, The Pennsylvania State University, University Park, PA 16802, USA

² School of Physics and Astronomy, University of Birmingham, Edgbaston, Birmingham, B15 2TT, UK

³ Department of Astronomy & Astrophysics, The Pennsylvania State University, University Park, PA 16802, USA

Received —

ABSTRACT

We consider a potentially new class of gravitational wave sources consisting of a white dwarf coalescing into a massive black hole in the mass range $\sim 10^4 - 10^5 M_\odot$. These sources are of particular interest because the gravitational wave signal produced during the inspiral phase can be detected by the *Laser Interferometer Space Antenna* (*LISA*) and is promptly followed, in an extended portion of the black hole and white dwarf mass parameter space, by an electro-magnetic signal generated by the tidal disruption of the star, detectable with X-ray, optical and UV telescopes. This class of sources could therefore yield a considerable number of scientific payoffs, that include precise cosmography at low redshift, demographics of black holes in the mass range $\sim 10^4 - 10^5 M_\odot$, insights into dynamical interactions and populations of white dwarfs in the cores of dwarf galaxies, as well as a new probe into the structure and equation of state of white dwarfs. By modelling the gravitational and electromagnetic radiation produced by these events, we find them detectable in both observational windows at a distance ≈ 200 Mpc, and possibly beyond for selected regions of the parameter space. We also estimate the detection rate for a number of model assumptions about black hole and white dwarf mass functions and dynamical interactions: the rate is (not surprisingly) highly uncertain, ranging from $\sim 0.01 \text{ yr}^{-1}$ to $\sim 100 \text{ yr}^{-1}$. This is due to the current limited theoretical understanding and minimal observational constraints for these objects and processes. However, capture rate scaling arguments favor the high end of the above range, making likely the detection of several events during the *LISA* lifetime.

Key words: black hole physics white dwarfs gravitational waves galaxies: dwarf radiation mechanisms: general

1 INTRODUCTION

The simultaneous detection of sources in both the electro-magnetic band - which provides a measurement of the source redshift, z - and the gravitational wave (GW) window - which yields a direct determination of the luminosity distance D_L to the source - could revolutionize cosmography by determining the distance scale of the Universe in a precise, calibration-free way. This was pointed out initially by Schutz (1986) in the context of ground-based observations of GWs from coalescing compact binaries with the network of ground-based laser interferometers now in operation (Whitcomb 2008). The observational capability of space-based instruments such as the *Laser Interferometer Space Antenna* (*LISA*; Bender et al. 1998), which could observe many sources at high signal-to-noise ratio (SNR) and large redshift, has attracted much attention recently. Sev-

eral scenarios have been considered, primarily related to the identification of the host galaxy or galaxy cluster of massive black hole (MBH) binary systems detected in GWs (Cutler 1998; Hughes 2002; Menou 2003; Vecchio 2004; Holz & Hughes 2005; Lang & Hughes 2006, 2008; Kocsis et al. 2006, 2007a,b; Arun et al. 2007; Cornish & Porter 2008; Trias & Sintes 2008), and the possible electro-magnetic signatures produced by the pre-glow/afterglow of the MBH mergers (Milosavljević & Phinney 2005; Dotti et al. 2006). The main obstacles to such groundbreaking observations are either the possible paucity of sources likely to produce significant gravitational and electro-magnetic radiation detectable to cosmological distances and/or the rather poor angular resolution of GW instruments (e.g. Cutler 1998; Hughes 2002; Vecchio 2004; Lang & Hughes 2006; Arun et al 2007; Cornish

& Porter 2008; Trias & Sintes 2008), which could inhibit the electro-magnetic identification of the host.

In this paper, we discuss a new class of GW sources that have received little attention so far (Menou, Haiman & Kocsis 2008): the inspiral of a white dwarf (WD) around a MBH in the mass range $\sim 10^4 - 10^5 M_\odot$ followed by the tidal disruption of the star before it plunges into the MBH. As we will show, these sources may be observable at low redshift (a few hundreds Mpc) with *LISA* and their electro-magnetic emission may be detectable with X-ray observatories and optical ground based telescopes. From the GW point of view, a MBH-WD binary is a different flavour of the so-called Extreme-Mass Ratio Inspirals or EMRIs. Traditionally, the fiducial EMRI is taken to be a stellar-mass $\sim 10 M_\odot$ black hole orbiting a $10^6 M_\odot$ MBH (Barack & Cutler 2004). The key difference between a "traditional EMRI" and a MBH-WD system considered in this paper is that for a range of MBH and WD masses, the inspiral does not proceed all the way until the compact object falls into the MBH horizon, but it terminates with the tidal disruption of the WD producing an electro-magnetic signature (for a MBH mass $\gtrsim 3 \times 10^5 M_\odot$, a WD survives throughout the whole inspiral and the system behaves just like a traditional EMRI). The observation of both gravitational and electro-magnetic signals from the same source provides a direct and calibration-free measurement of the $D_L(z)$ relationship and opens new avenues for cosmography and, more directly (due to the low redshift of most of the expected sources) a completely independent determination of the Hubble parameter H_0 that does not depend on any distance calibration. This class of sources can also provide new insights into a number of unanswered questions in relativistic astrophysics: (i) the demographics of MBHs in the mass range $\sim 10^4 - 10^5 M_\odot$ – only a handful of MBH candidates with masses below $10^6 M_\odot$ (Greene & Ho 2004; Barth, Greene & Ho 2005) is known to date, their mass estimate is rather uncertain, since it is based on the emission-line spectra of the active nuclei, and none of them have masses below $10^5 M_\odot$ – (ii) the populations of WDs and the dynamical processes that take place in the cores of dwarf galaxies, that are unknown and unconstrained by observations, and (iii) the structure and equation of state of WDs – the exact point at which tidal disruption occurs indeed depends on the WD equation of state (e.g. Magorrian & Tremaine 1999), and the electro-magnetic signature carries information about the WD composition.

The paper is organized as follows: in Section 2 we identify the mass range of WDs and central MBHs that lead to the tidal disruption of the star before it plunges onto the black hole and we determine the volume of the Universe that *LISA* will be able to survey; in Section 3 we derive the GW detection rate of these sources and discuss its uncertainties; in Section 4 we model the electro-magnetic counterpart to MBH-WD EMRIs; finally, in Section 5 we summarize the main results and our conclusions.

2 THE GRAVITATIONAL WAVE SIGNAL

2.1 Mass parameter space

Let us consider a MBH of mass M and an inspiralling WD of mass m and radius r . The tidal disruption radius of the WD is:

$$R_{\text{td}} = \left(\eta^2 \frac{M}{m} \right)^{1/3} r, \quad (1)$$

where η is a factor of order unity that depends on the star equation of state (for sake of simplicity we set $\eta = 1$ in our analysis). R_{td} can be expressed as a function of only m and M once the WD $m(r)$ relation is fixed. Here we use a polytrope approximation with $\Gamma = 5/3$ (Nauenberg 1972):

$$r = 8 \times 10^8 \text{ cm} \left(\frac{M_{\text{CH}}}{m} \right)^{1/3} \mathcal{F}^{3/4}(m), \quad (2)$$

where $\mathcal{F}(m) = 1 - (m/M_{\text{CH}})^{4/3}$ and $M_{\text{CH}} \simeq 1.44 M_\odot$ is the Chandrasekhar mass. There are two characteristic length scales (and associated frequencies) that one needs to consider with respect to the tidal radius. The first is the orbital separation R_{LSO} corresponding to the *last stable orbit* where the binary encounters a dynamical instability and there is a transition from the adiabatic inspiral to the freely falling plunge; for an inspiral onto a Schwarzschild MBH $R_{\text{LSO}} = M(6 + 2e_f)/(1 + e_f)$, where e_f is the eccentricity of the orbit at the plunge, and we have adopted geometrical units, in which $c = G = 1$. The second is the separation R_{H} at which the WD falls into the MBH horizon, or, in other words, the merged binary forms a common horizon and the system settles down through the ringing of a Kerr MBH. For a Schwarzschild MBH $R_{\text{H}} = 2M$.

We can therefore distinguish the following three cases:

(i) $R_{\text{td}} > R_{\text{LSO}}$: the star is disrupted before the last stable orbit. The in-spiral is interrupted generating a distinct electro-magnetic signature observable both in X-ray and in Optical/UV that we will describe in detail in Section 4.

(ii) $R_{\text{H}} < R_{\text{td}} < R_{\text{LSO}}$: the star is disrupted during the merger phase but before it falls into the BH horizon: the inspiral phase is essentially unchanged with respect to the "standard EMRI" evolution. Whether an object disrupted while plunging would leave any identifiable electro-magnetic signature is an open question that we will not try to address in this work. In the following we will derive event rates with and without including this possibility.

(iii) $R_{\text{H}} > R_{\text{td}}$: the dynamical evolution is indistinguishable from the "traditional" EMRIs considered in the literature so far, and the only trace that the compact object is a WD is entirely contained in the measurement of the compact object mass through the observation of the GW signal evolution. No electro-magnetic signal is expected.

Our analysis is focused on events that may produce an electro-magnetic counterpart, through the tidal disruption of a WD; we will therefore restrict our attention to the scenarios (i) and (ii). In the following we will start by considering a WD orbiting a Schwarzschild MBH; we discuss the impact of spins on the results in Section 2.3. Setting R_{td} equal to R_{LSO} and R_{H} , respectively, we find the two critical black masses that mark the transition between the three cases:

$$M \simeq 3.3 \times 10^4 M_\odot \left(\frac{1 + e_f}{1 + e_f/3} \right)^{3/2} \left(\frac{m}{M_\odot} \right)^{-1} \mathcal{F}^{3/4}(m), \quad (3)$$

$$M \simeq 1.7 \times 10^5 M_\odot \left(\frac{m}{M_\odot} \right)^{-1} \mathcal{F}^{3/4}(m). \quad (4)$$

Clearly, the more massive the MBH, the lighter the WD in order to have tidal disruption before the star plunges into the

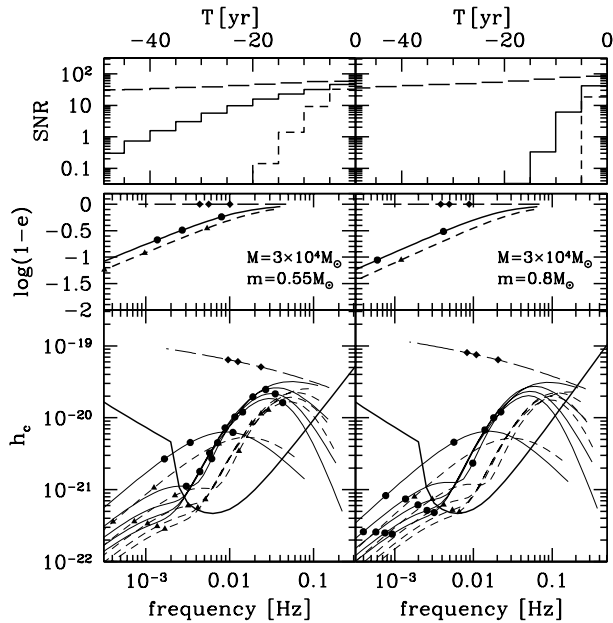


Figure 1. SNR build-up during the last years of inspiral for two different WD and MBH mass combinations at a luminosity distance of 100 Mpc. In each panel, long-dashed lines are for a WD with $e_f = 0$ (i.e. in circular orbit), solid lines are for $e_f = 0.1$ and short-dashed lines are for $e_f = 0.2$. *Lower panels:* characteristic amplitude h_c of the signal versus observed frequency (for eccentric binaries the first five harmonics are plotted). The points mark, from right to left, the frequency emitted at 1, 5 and 10 yr before the WD reaches the maximum between R_{td} and R_{LSO} . The thick solid line is the *LISA* sensitivity with the galactic WD-WD confusion noise (according to the prescription given by BC04) taken into account. *Middle panels:* eccentricity of the binary versus the orbital frequency. *Upper panels:* SNR integrated in different 5-yr observation bins before the final coalescence.

MBH horizon. Surveys of this class of EMRIs will therefore probe the MBH mass function in the range $\sim 10^4 - 10^5 M_\odot$. Notice that neutron stars are disrupted by black holes with masses of the order of tens of solar masses: gravitational radiation is emitted in the frequency window accessible through ground-based laser interferometers (e.g. Vallisneri 2000) and we will therefore not consider these sources in this paper.

2.2 Observable volume

Having identified the region of interest in the mass plane, we can now compute the volume of the Universe that will be accessible to *LISA*. We begin by computing the (angle-averaged) SNR at which *LISA* will be able to observe a system at a fiducial luminosity distance that we set to $D_L = 100$ Mpc. The SNR scales as $1/D_L$ and, once we specify the minimum SNR needed for detection, it is straightforward to quantify the depth of *LISA* surveys as a function of the source parameters. We model the EMRI waveforms according to Barack & Cutler (2004; hereafter BC04), therefore adopting what are known as “analytic kludge” waveforms: the orbits are instantaneously approximated as Newtonian ellipses and gravitational radiation is given by the corresponding Peters and Mathews formula (Peters &

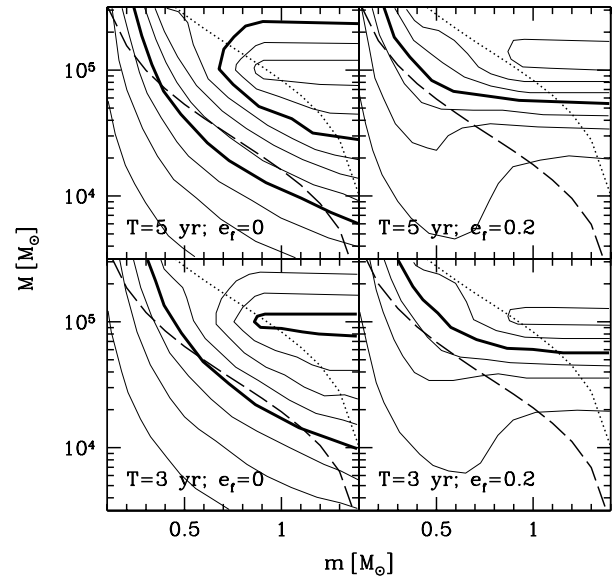


Figure 2. Contour plot of D_{MAX} assuming a detection threshold corresponding to $\text{SNR}=30$ and for two different choice of observation time – $T = 3$ and 5 yr – and final eccentricity, $e_f = 0$ and 0.2 . In each panel, the thin contours are placed every 50 Mpc with distance increasing from the bottom-left to the top-right; the thick contours label 200 Mpc and 400 Mpc. MBH-WD binaries below the dashed line result in the WD disruption before the last stable orbit, and an electro-magnetic counterpart is expected (see Section 4). For MBH-WD systems between the dashed and the dotted lines, the WD is disrupted during the final plunge, *before* crossing the MBH event horizon.

Mathews 1963; Peters 1964), but perihelion direction, orbital plane, semi-major axis and eccentricity evolve according to post-Newtonian equations. The signal is generated by integrating backward in time Equations (28–30) of BC04 starting from the orbital frequency emitted at the minimum allowed orbital separation. The latter is set to be the larger between the last stable orbit and the tidal disruption radius of the WD. The angle-averaged SNR is computed following the prescription described in Section 5 of BC04, assuming observations with the two Michelson-like observables. For a given distance and observation time T , the SNR is determined by M , m and e_f . We sample M between $10^{3.5} M_\odot$ and $10^6 M_\odot$ at intervals of $\log M = 0.5$, m on a grid of $0.1 M_\odot$ between $0.1 M_\odot$ and $1.4 M_\odot$, and we consider four values for the final eccentricity: $e_f = 0, 0.1, 0.2, 0.3$. The remaining parameter that affects the SNR is the duration of the observation T ; here we consider $T = 3$ and 5 yr.

In figure 1 we show examples of the expected GW signal and of the eccentricity and the SNR evolution as a function of the observation time. We show, in particular, the characteristic amplitude $h_{c,n} \propto \dot{E}_n / f_n$ – here \dot{E}_n is the energy emitted per unit time in the n -th harmonic with observed frequency $f_n = n\nu + \dot{\gamma}/\pi$, where γ is a precession angle (see BC04) and \dot{f}_n is the time derivative of f_n – of the first five harmonics as a function of frequency and the evolution of eccentricity of the fiducial systems (for $e = 0$ only the harmonics corresponding to $n = 2$ contributes to the signal). Notice that EMRIs characterised by $e = 0$ produce larger

SNR than those with $e \neq 0$. In fact the SNR accumulated in the last few years of the life of a source decreases with increasing eccentricity due to the steep increase of f_n as a function of e , and the increase of the *LISA* noise at frequencies above ≈ 5 mHz. Circular EMRIs can also be detected at a fiducial distance of 100 Mpc with a SNR $\gtrsim 30$ several tens of years before coalescence/disruption. This is not the case for eccentric systems, because the peak of their emission is moved progressively away from the “sweet-spot” of the *LISA* sensitivity window. For systems characterized by a non-negligible eccentricity at disruption $e \sim 0.1$, those with $m \sim 0.5 M_\odot$ produce the highest SNR.

At this stage we still do not have a sufficiently detailed understanding of any end-to-end analysis algorithm for the detection of EMRIs, and therefore it is impossible to adopt a precise value for the SNR threshold at which detection can be achieved. Here we will adopt SNR= 30, following Gair et al. (2004), a value consistent with the performance of the very first implementation of algorithms being explored within the Mock *LISA* Data Challenges (e.g. Babak et al. 2008; Gair et al. 2008a,b; Cornish 2008). After setting the detection threshold, it is straightforward to compute the maximum luminosity distance D_{MAX} at which a source can be detected as a function of masses and eccentricity (for a given observation time). Contour plots of D_{MAX} in the (M, m) plane and for $e_f = 0, 0.2$ are shown in figure 2 assuming $T = 3$ and 5 yr. It is clear that circular binaries are likely to be detected at much larger distances than systems characterised by $e_f \neq 0$. In the case $e_f = 0$ there is a small region of parameter space for which the WD is disrupted before the last stable orbit and is observable up to $D_{\text{MAX}} \simeq 200 - 250$ Mpc. If we assume that a WD disrupted during the final plunge would also yield a detectable electro-magnetic burst, then *LISA* could probe even deeper, possibly reaching $D_{\text{MAX}} \simeq 450$ Mpc. As a general trend, for fixed source masses the volume of the universe surveyed by *LISA* decreases with increasing e_f . For example, if $e_f = 0.2$, the maximum distance at which *LISA* can detect a MBH-WD binary leading to WD disruption before the last stable orbit is ≈ 150 Mpc. D_{MAX} obviously increases with observation time, however, even with only $T = 1$ yr *LISA* can reach $D_{\text{MAX}} \gtrsim 100$ Mpc. We will use the values of D_{MAX} derived in this section to obtain estimates of the *LISA* detection rates of GWs from MBH-WD leading to the disruption of the WD in Section 3. The detection rate scales as D_{MAX}^3 and any uncertainty in the determination of the maximum distance will be reflected accordingly in the rates.

2.3 The role of black hole spin

The previous results were obtained assuming a Schwarzschild MBH. If MBHs are rapidly rotating, as our present astrophysical understanding suggests (e.g. Shapiro 2005), then relativistic spin-orbit coupling affects the evolution of the binary and the resulting GW signal. To quantify the impact of spins on the range of MBH-WD systems observable with *LISA* with respect to the non-spinning case considered in the previous Section we consider two extreme cases: in both instances the MBH is almost maximally rotating (the spin parameter is set to $a = 0.99$), the WD orbit is equatorial, but in one case it is prograde and in the other it is retrograde. The MBH spin affects the

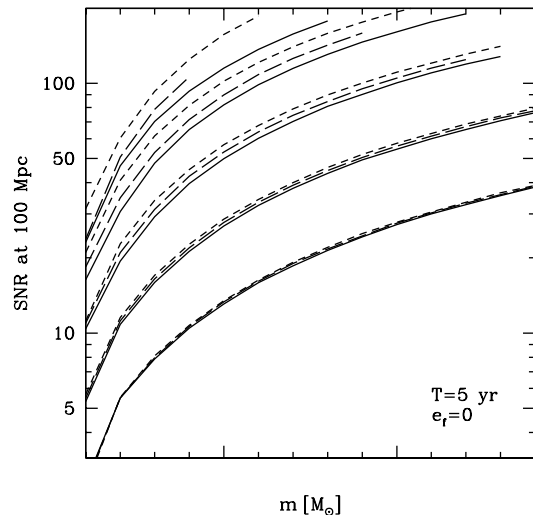


Figure 3. SNR obtained with 5 yr of coherent integration before the maximum between R_{td} and R_{LSO} . The WD is assumed to orbit a Kerr MBH with $a = 0.99$ either in an equatorial prograde (solid lines) or retrograde (short-dashed lines) orbit, or a Schwarzschild MBH (long-dashed lines). Each series of curves (solid, long-dashed or short-dashed) refers, from bottom to top, to WDs orbiting around a MBH with $M = 10^{3.5}, 10^4, 10^{4.5}, 10^5, 10^{5.5} M_\odot$.

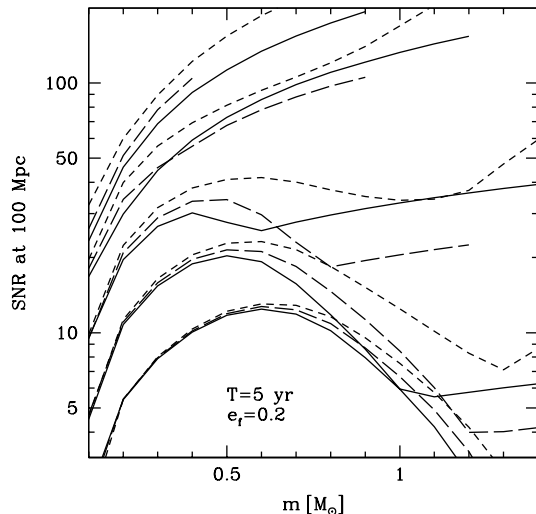


Figure 4. Same as figure 3 but for systems with non negligible final eccentricity. Line-style and curve sequences as in figure 3.

signal – and ultimately the detection rate – in two ways: (i) the strength of the emitted gravitational radiation, and (ii) the distance at which a WD is tidally disrupted. The emitted GW amplitude is larger for prograde orbits and so is the SNR (see figures 3 and 4). This is a zero-to-40% effect increasing with the BH mass, and favors the detection of prograde orbits. However, the location of the last stable orbit also shifts: for an equatorial prograde orbit, the LSO is at $R = M$; in this case the WD is either disrupted during

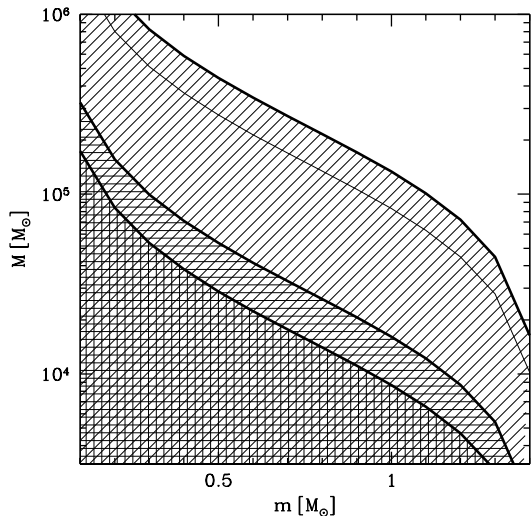


Figure 5. The mass parameter space of MBH-WD binary systems. The thick solid lines mark the combination of MBH and WD mass for which the tidal disruption radius R_{td} equals the radius of the last stable orbit R_{LSO} . From top to bottom they refer to: a prograde orbit around a Kerr MBH with $a = 0.99$, an orbit around a Schwarzschild MBH, and a retrograde orbit around a Kerr MBH with $a = 0.99$. The shaded area(s) below the curves represent the portion of the $M - m$ plane for which WD disruption occurs before the LSO and an electro-magnetic counterpart is expected. For comparison, the thin line represents the mass combinations for which R_{td} equals the radius of the horizon ($2M$) for a Schwarzschild MBH.

the inspiral phase or simply plunges into the MBH horizon without producing any electro-magnetic signature. For an equatorial retrograde orbit, the LSO is located at $R = 9M$; in this case the region where the WD could be disrupted during the final plunge before entering the BH horizon is much wider. We found that this LSO shift has a small influence on the SNR (the essential point is that radiation generated when the orbital frequency is close to the LSO, whether it is located at M or $9M$, is detected in a region of the *LISA* observational window where the sensitivity is already compromised by the fact that the instrument arm-length is significantly longer than the typical GW wavelength; see figure 1), however, it strongly affects the portion of the $M - m$ parameter space in which the WD tidal disruption occurs outside the LSO, as shown in figure 5. The prograde LSO for a MBH with $a = 0.99$ is located at a much smaller radius, increasing the maximum MBH mass that allows WD disruption *before* the final plunge. For example, a $0.5 M_{\odot}$ WD is disrupted outside the LSO of a Schwarzschild MBH of $M < 5 \times 10^4 M_{\odot}$; however, if the same WD is in an equatorial prograde orbit around a Kerr BH with $a = 0.99$, it is disrupted outside the LSO if $M < 5 \times 10^5 M_{\odot}$. In this latter case disruption caused by more (and more massive, i.e. detectable to larger distances) MBHs is observable both in the gravitational wave window and in the electro-magnetic band, yielding a much higher event rate. For retrograde orbits, the LSO is larger – $R_{LSO} \approx 9M$ – and the WD is disrupted by MBHs of smaller masses (see figure 5). However, WDs will be captured in

random direction with respect to the MBH spin axis, and the detection rate will tend to increase on average, since what it is gained in terms of SNR and of available mass parameter space because of the prograde orbits is much more than what it is lost because of the retrograde ones. We therefore use as a reference for rate estimations the non spinning MBH case, as this sets a lower limit to the detection rate.

3 DETECTION RATE

We can now address the *LISA* detection rate of inspirals signals from MBH-WD binaries in which the WD is disrupted before falling into the MBH horizon. The detection rate Γ can be computed via

$$\Gamma = \int dm \int dM \frac{d^2 n}{dM dm} V(M, m), \quad (5)$$

where $V(M, m) = 4/3\pi D_{MAX}^3(M, m)$ is the observable volume – here we consider an Euclidean approximation, due to the low redshift of the sources covered by the instrument, see Section 2 and figures 2, 3 and 4 – and

$$\frac{d^2 n}{dM dm} = \frac{dn}{dM} \times \left. \frac{d\Gamma}{dm} \right|_M. \quad (6)$$

The detection rate depends sensitively on two rather unknown quantities: the local number density of MBHs per unit mass dn/dM , and the WD inspiral rate per unit WD mass $d\Gamma/dm|_M$, given the MBH mass. The factorization in equation (6) is based on the simplifying assumption that the inspiral rate is a function of the MBH mass only, i.e., we are assuming that MBHs with the same mass are embedded in similar stellar cusps.

At present there are no stringent constraints on dn/dM in the mass range of interest ($M \lesssim 3 \times 10^5 M_{\odot}$). The MBH mass function was derived by Aller & Richstone (2002) for $M > 10^6 M_{\odot}$ by combining the galaxy luminosity function with the Faber-Jackson and the $M - \sigma$ relations. The slope of the faint end of the luminosity function is, however, controversial. Some works suggest that in clusters and groups of galaxies it can be as steep as $L^{-1.8}$ (where L is the luminosity) for magnitudes brighter than -18 (e.g. Wilson et al. 1997; Sabatini et al. 2003; Gonzalez et al. 2006). In contrast, Trentham & Tully (2002) find a scaling of $L^{-1.2}$ in the magnitude range $[-18, -10]$. The lack of information on the faint-end slope of the luminosity function implies an uncertainty of a factor of ~ 10 on the number density of MBHs in the range $10^4 M_{\odot} \lesssim M \lesssim 10^5 M_{\odot}$, even assuming that the Faber-Jackson and the $M - \sigma$ relations can be extrapolated to such small galaxies. This highlights the role that *LISA* observations could play in providing information on the demographics of MBHs in this mass range that has been proven difficult to probe so far, and on their host galaxies.

Estimates of the WD inspiral rate onto a MBH embedded in a stellar cusp are even more uncertain and they span several orders of magnitude. Let us define the total rate for a single MBH as

$$\Gamma|_M = \int \left. \frac{d\Gamma}{dm} \right|_M dm. \quad (7)$$

. We assume for simplicity that the differential rate is $d\Gamma/dm|_M = \Gamma|_M p_{\text{WD}}$, where p_{WD} is the WD mass density function taken from Madej, Nalezyty & Althaus (2004). In dense environments like compact star clusters or dwarf galaxy nuclei (where we expect to find MBHs in the mass range of interest), MBH-WD binaries can be generated primarily by (i) two body scattering diffusion of stars into the MBH loss cone, and (ii) tidal break-up of a stellar binary followed by the capture of one of the components. The former is likely to generate EMRIs with non-negligible final eccentricity, while the latter is likely to generate EMRIs with $e \approx 0$ (Miller et al. 2005; see Amaro-Seoane et al. 2007 for a review). Estimates of the capture rate due to the two body scattering processes have been typically carried out for a fiducial MBH mass $\sim 10^6 M_\odot$, and the results then rescaled to other MBH masses. Hils & Bender (1995) and Ivanov (2002) find rates in the range $5 \times 10^{-9} < \Gamma|_M < 2 \times 10^{-8} \text{ yr}^{-1}$. Ivanov (2002) suggested a scaling $\propto M^{-1}$. Results obtained by Sigurdsson & Rees (1997) span several orders of magnitude, depending on the radial density profile of the stellar distribution. For typical observed power-law profiles $\rho_{\text{pl}} \propto r_{\text{pl}}^{-1.5, -2}$, they suggest $10^{-10} < \Gamma|_M < 5 \times 10^{-7} \text{ yr}^{-1}$. Hopman & Alexander (2006a), taking into account mass segregation, give $\Gamma|_M \approx 3 \times 10^{-8} \text{ yr}^{-1}$ for a Milky Way MBH. This number can be larger by a factor ≈ 10 if resonant relaxation is efficient (Hopman & Alexander 2006b). They also estimate a scaling $\propto M^{-0.25}$. Monte Carlo simulations performed by Freitag (2001) give rates as high as $5 \times 10^{-6} \text{ yr}^{-1}$ for a Milky Way MBH, and Gair et al. (2004) infer a mass scaling $\propto M^{3/8}$ on the basis of dynamical friction arguments. On the other hand there are currently no detailed calculations of the rate of EMRIs generated through tidal break-up, but there are clues suggesting that it could even exceed the rate yielded by standard relaxation processes (Miller et al. 2005; Alexander 2007).

It is clear that the theoretical understanding of the magnitude and mass scaling of $\Gamma|_M$ is quite poor, which highlights once more the potential impact of *LISA* observations of this class of objects. The actual rate for $M < 10^6 M_\odot$, which is of interest here, depends both on how the rates scale with M and on how the properties of the nuclear cluster scale with M . Observational data for the small dense clusters associated with low mass nuclei are sparse. If the observed inverse correlation between M and the stellar density in the nucleus holds for these lower masses, then we expect the rates to be 3–10 times larger (10^{-7} – 10^{-6} yr^{-1}) with respect to a $10^6 M_\odot$ MBH, taking the overlap of recent estimates and scaling, which ultimately favors detection rates at the upper end of the range we will estimate below. It is also possible that the stellar zero-age mass function is systematically skewed to higher masses in galactic nuclei, in which case the median WD mass may be higher than estimated from the field mass function, perhaps as high as 0.7 – $0.8 M_\odot$, and the ratio of WDs to current main sequence stars would be significantly higher. This may enhance the rate by another factor of several due to stronger scattering. On the other hand, mass segregation effects might lower the rates, as the mean stellar mass in the nucleus would also be significantly higher.

The detection rates of WD-MBH binaries leading to the tidal disruption of the WD companion derived using equation (5) lie in the range $0.01 \text{ yr}^{-1} \lesssim \Gamma \lesssim 100 \text{ yr}^{-1}$ and are

	Detection rates [yr^{-1}]			
	pessimistic		optimistic	
	$e_f = 0$	$e_f = 0.2$	$e_f = 0$	$e_f = 0.2$
Schw no plunge	0.03	0.01	21	4
Schw plunge	0.15	0.03	71	21
Kerr prograde	0.45	0.40	163	124

Table 1. Detection rates (events/yr) considering a 5 yr signal integration under different assumptions for MBH spins and WD orbits. The ‘Schw no plunge’ case assumes an event to be detectable both in the gravitational and electro-magnetic bands only if the WD tidal disruption occurs outside the last stable orbit, while in the ‘Schw plunge’ case we assume a visible electro-magnetic counterpart also if disruption takes place during the final plunge. The pessimistic and optimistic scenarios are described in the text.

summarised in table 1. Optimistic estimates are calculated assuming the WD disruption rate quoted by Freitag (2001) with the Gair et al. (2004) mass scaling coupled with a steep faint end of the MBH mass function $dn/d\log M \propto M^{-1}$ (e.g. Gonzalez et al. 2006); these assumptions lead to ~ 5 – 150 events per year, depending on MBH spin, WD eccentricity, and the assumption that an electro-magnetic counterpart exists when the WD is disrupted outside the black hole horizon, and not simply before the last stable circular orbit. Pessimistic estimates rely on WD disruption rates derived by Hopman & Alexander (2006b), in which no mass segregation or resonant relaxation effects are taken into account, coupled with a flat extrapolation of the MBH mass function ($dn/d\log M = \text{const.}$, Aller & Richstone 2002), and are in the range ~ 0.01 – 0.5 yr^{-1} . It is then likely that *LISA* (assuming a five years operation lifetime) would observe several of these MBH-WD sources. Detection rates for some fiducial cases are summarised in Table 1. Note that the presence of binaries with $e \approx 0$ could be decisive for successful *LISA* detections, because circular systems can be detected to significantly larger distances (see figure 2) and the associated rates are much higher, as shown in table 1.

4 ELECTROMAGNETIC COUNTERPARTS

In this section we model the electro-magnetic signature of a WD disrupted *outside* the last stable orbit and discuss the prospects for observing such events. Whether a disruption during the final plunge would lead to any distinct electro-magnetic signal, is still an open question that would require full relativistic hydrodynamical simulations, that go beyond the scope of this paper and will not be addressed here.

The prompt electro-magnetic signature of the disruption of a WD from a MBH consists of an energetic flare that appears when accretion begins and lasts while accretion fuel is available. Since the orbit decays very quickly via gravitational radiation, the only limitation to the accretion rate is the Eddington limit. Thus, the bolometric luminosity can be written as $L_{\text{bol}} = 1.3 \times 10^{43} (M/10^5 M_\odot) \text{ erg s}^{-1}$. The corresponding accretion rate is $\dot{M} \approx 2 \times 10^{-3} (\epsilon/0.1)^{-1} (M/10^5 M_\odot) M_\odot \text{ yr}^{-1}$, where ϵ is the efficiency of conversion of the rest energy of the accreting matter to radiation. At this rate, a CO WD with

a mass of $0.55 M_{\odot}$ will be consumed in about 300 years. Flares with such luminosities can be easily detected with present-day X-ray observatories out to the distance of the Coma cluster (~ 100 Mpc). By analogy with the results of Rantsiou et al. (2008) who compute the tidal disruption of a neutron star by a $10 M_{\odot}$ black hole, we expect that a portion of the post-disruption debris will become unbound and expand radially outwards with a morphology resembling an arc. Photoionization of this arc of debris by the accretion-powered X-rays and UV light will lead to the emission of optical lines. The late-time afterglow spectrum of the debris makes up a very distinct signature of such an event.

In order to calculate the emission-line strengths from the photoionized debris, we first estimate how its physical properties will evolve with time. We assume that the debris arc contains a small fraction, of order 10%, of the mass of the WD and it is launched from the tidal disruption radius at the escape speed. As the debris expands, it remains primarily in the original orbital plane but also expands perpendicularly to it at the speed of sound c_s . Because of photoionization, the excitation temperature of the electrons in the debris remains relatively steady at $T \sim$ a few $\times 10^4$ K, thus $c_s \approx 10 (T/10^4 \text{ K})^{1/2} \text{ km s}^{-1}$ (this is based on the photoionization calculations that we describe in the next paragraph). As fiducial case we consider a $0.55 M_{\odot}$ CO WD disrupted by a $10^5 M_{\odot}$ MBH. This WD mass represents the peak of the mass distribution found by Madej, Należyty & Althaus 2004), and such WD-MBH combination would lead to the disruption of the star for mildly spinning MBHs and prograde orbits, and the GW precursor would be detectable well beyond 200 Mpc. We also consider briefly the emission-line spectrum from the disruption of a $0.4 M_{\odot}$ He WD, which is a less likely event. The tidal disruption radius of the CO WD is $R_{\text{td}} = 5.3 \times 10^{10} \text{ cm}$ and the dynamical time at this radius is $t_{\text{dyn}}(R_{\text{td}}) = 2.4 \text{ s}$. Under the above assumptions, at $t \gg t_{\text{dyn}}(R_{\text{td}})$, the radius of the debris increases with time as $r_d(t) \propto t^{2/3}$ and reaches $9 \times 10^{13} \text{ cm}$ after approximately 31 hours. Accordingly, the density of the debris evolves as $\rho_d(t) \propto t^{-7/3}$ and the column density through the debris (along the orbital plane) decay as $t^{-5/3}$. The solid angle subtended by the arc of debris to the continuum source *increases* with time as $t^{1/3}$ because the expansion rate at the speed of sound perpendicular to the plane of the orbit is slightly faster than the expansion in the orbital plane.

To compute the ionization structure and emission properties of the debris, we used the photoionization code Cloudy (Ferland et al. 1998), which computes the thermal and ionization balance of the debris in detail, taking into account a wide variety of physical processes and emission mechanisms. The ionization level of the gas is described by the ionization parameter $U_H = Q_H/(n_H r_d^2 c)$, where $Q_H = \int_{1 \text{ Ry}}^{\infty} (L_{\nu}/h\nu) d\nu$ is the emission rate of hydrogen-ionizing photons by the central accreting MBH, n_H is the hydrogen number density in the debris and r_d is its distance from the central source of ionizing photons. In this particular case, we must re-define the ionization parameter because hydrogen is very sparse in the photoionized debris. We choose oxygen as the reference element instead because it makes up most of the mass in the debris and because its first ionization potential happens to be nearly identical to that of hydrogen. The two ionization parameters are related

by $U_O = (m_H A_O/m_O)U_H$, where m_H and m_O are hydrogen and oxygen masses, respectively, and $A_O = 16$ is the mass number of oxygen. Thus, $U_O = U(t) \propto L(t)/[\rho_d(t)r_d^2(t)]$. We make the assumption that the accretion rate, hence the ionizing luminosity, remains steady at the Eddington limit in the immediate aftermath of the disruption, implying that $U(t) \propto t$. The composition of the debris is a crucial ingredient of the calculation. Following Madej et al. (2004), we assume that the mass of the CO WD consists of 67 % of O, 32 % of C, 1 % of He, 0.001% of H, and other metals in the mass fractions observed in the Sun (Anders & Grevesse 1989). We note that this composition is consistent with WD astroseismology results (Metcalf 2003; Staniero et al. 2003). We adopted the Mathews & Ferland (1987) model for the spectral energy distribution of the ionizing continuum, which is motivated by observations of quasars. This model comprises a hard power-law in the X-ray band and an excess of UV photons (a "UV bump").

The photoionization calculations predict an emission spectrum of C and O recombination lines, as one would expect. We have calculated models at 1, 2, 4, 7, 14, 21, and 28 days after the event, which show that the ionization parameter increases from $\log U_O = -5.8$ at ~ 1 day after the event to $\log U_O = -4.4$ at 4 weeks after the event, as the debris expands and thins out. The strongest oxygen and carbon lines in the optical spectrum are O II $\lambda 4341$, O I $\lambda 4368$, O I $\lambda 8446$, O II $\lambda 4651$, and C I $\lambda 8727$. In addition the Ca II H&K doublet ($\lambda\lambda 3934, 3969$) and the N I $\lambda 3466$ line appear to be strong. The evolution of the optical lines with time is shown in Figure 6. In the near-UV part of the spectrum, the strongest lines are from carbon, e.g., C II $\lambda 1335$, C I $\lambda 1656$, C I $\lambda 1248$, C IV $\lambda\lambda 1548, 1551$, and silicon, namely Si III $\lambda 1207$, Si II $\lambda 1263$, Si IV $\lambda\lambda 1394, 1403$. The evolution of the near-UV lines with time is shown in Figure 7. The behavior seen in different lines, i.e., the fact that specific lines rise with time while other fall, constitutes a diagnostic test for identifying this type of event.

The behavior of the spectrum of helium-rich debris from the disruption of a $0.4 M_{\odot}$ WD is qualitatively similar. The strong optical emission lines are primarily from helium, and include He I $\lambda 5876$, $\lambda 4026$, and $\lambda 4471$ and He II $\lambda 3203$, $\lambda 4686$, and $\lambda 5412$. The He II lines are predicted to rise with time relative to the He I lines. In the near-UV band, the strong lines are the same as those of the CO WD case, with the addition of one strong helium line, He II $\lambda 1640$. The characteristic behavior we predict in the UV band is that the C II $\lambda 1335$, Si IV $\lambda\lambda 1394, 1403$ and Si III $\lambda 1207$ lines decline with time relative to He II $\lambda 1640$.

Our emission-line luminosity estimates are subject to uncertainties in the distribution of the post-disruption debris and the evolution of ionizing luminosity with time (we have assumed the ionizing luminosity to be steady during the first month after the event). Nevertheless, an interesting feature of our predicted luminosity evolution is the increase in the luminosity of some of the strong emission lines with time. This is a consequence of the fact that the excitation rate of these lines increases as the density of the debris drops allowing the ionizing photons to penetrate deeper into the debris. Taking these luminosity estimates at face value, we expect that the optical emission lines should be detectable out to the distance of the Virgo cluster (~ 16 Mpc) with a few-hour exposure on a 4m-class telescope, and well beyond

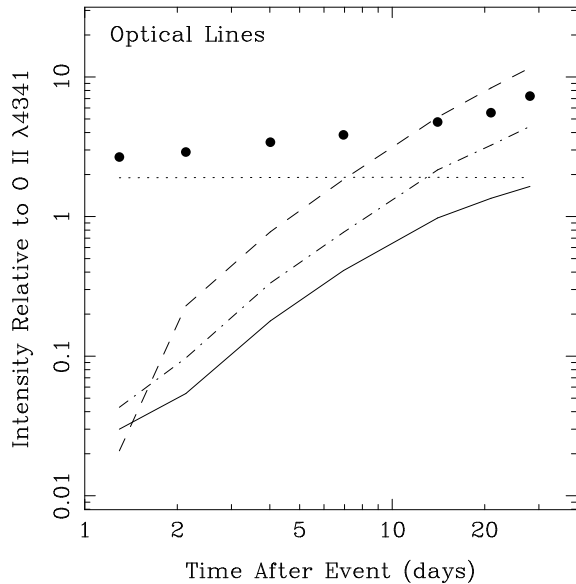


Figure 6. Time evolution of the intensities of selected, strong, optical emission lines relative to O II $\lambda 4341$. Solid line – O I $\lambda 4368$; dashed line – C I $\lambda 8727$; dotted line – O II $\lambda 4651$; dot-dashed line – Ca II $\lambda 3934$. The large filled circles show the evolution of the luminosity of the reference line, O II $\lambda 4341$, in units of 10^{36} erg s $^{-1}$.

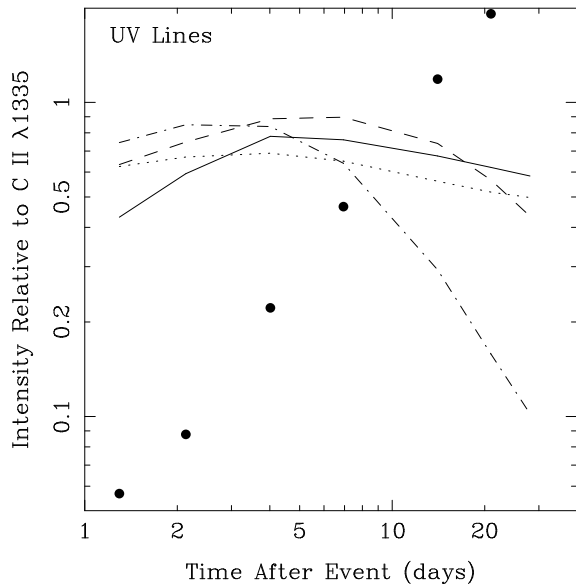


Figure 7. Time evolution of the intensities of selected, strong, ultraviolet emission lines relative to C II $\lambda 1335$. Solid line – C IV $\lambda 1551$; dashed line – C I $\lambda 1656$; dotted line – Si III $\lambda 1207$; dot-dashed line – C I $\lambda 1248$. The large filled circles show the evolution of the luminosity of the reference line, C II $\lambda 1335$, in units of 10^{36} erg s $^{-1}$.

the Coma cluster with a few hour exposure on a 30m-class telescope. The UV lines should be detectable out to the distance of the Virgo cluster with a telescope of the class of the *Hubble Space Telescope*. The capabilities of present and near future observatories should therefore allow the identification of the electro-magnetic counterpart associated to the

LISA detections gravitational waves of MBH-WD within the relevant parameter range.

5 SUMMARY

In this paper we have considered a class of *LISA* sources that have not been explored so far, consisting of a WD inspiralling onto a MBH in the mass range $\sim 10^4 - 10^5 M_{\odot}$. These sources are of particular interest because the gravitational wave signal produced during the inspiral can be detected with *LISA* and serves as a precursor for an electromagnetic flash – likely detectable in X-ray, and at optical and ultra-violet wavelengths – generated during the tidal disruption of the star and the subsequent distinctive accretion episode, which takes place for a considerable region of the mass parameter space. Observations of the same source in the gravitational and electromagnetic band enable an independent and calibration-free determination of the Hubble parameter at low redshift $z \lesssim 0.1$ (through the direct measurement of the redshift *and* luminosity distance of the same source), studies of the faint end of the MBH mass function in (dwarf) galaxies, measurements of the mass distribution function of extra-galactic WDs and in particular of those in galaxy cores, and provide a probe of the structure and equation of state of WDs, and of dynamical processes in the cores of galaxies.

We have determined the range of WD and MBH masses that lead to a tidal disruption before the final plunge, hence producing an electro-magnetic counterpart to the GW emission. In order to do so we have adopted a polytropic approximation of the WD mass-radius relation. In the future it is important to explore more sophisticated models to establish the dependence of the results presented here on this assumption. We have modelled the expected GW signal using “analytical kludge” waveforms *a-la* Barack & Cutler and have explored the dependence of the SNR on selected values of the eccentricity and the MBH spin. We found that the maximum distance at which *LISA* can observe these events depends both on the MBH spin and the orbital eccentricity, with circular prograde orbits around a highly spinning MBH producing signals observable to larger distances. A typical $0.5 M_{\odot}$ WD orbiting a $5 \times 10^4 M_{\odot}$ Schwarzschild MBH would be observable up to 200 Mpc, assuming a detection threshold equivalent to an optimal SNR of 30 in the two combined noise orthogonal unequal-arm Michelson observables for 5 years of integration.

Based on current (rather uncertain) estimates of the MBH population and of the rates at which they capture WDs we have computed the LISA detection rate and discussed its uncertainties. Circular binaries yield a higher detection rate (by up to a factor of ~ 3) with respect to eccentric ones, due to their higher SNR. A substantial population of highly spinning MBH would enhance the detection rate, since the last stable circular orbit of a WD inspiralling on a prograde orbit would be much smaller. More massive (i.e. observable to further distances) MBHs would enhance the detection rate. The rates that we obtain span almost four orders of magnitude, from 0.01 to 100 events per year and are listed in table 1. Scaling arguments for the stellar density in galactic centers suggest high WD disruption rates, up to 10^{-6} yr $^{-1}$, in dwarf nuclei favoring the upper end of the

detection rate range quoted above. Assuming a minimum lifetime of 5 yrs, *LISA* will likely see several of these events.

We have also modeled the electro-magnetic signature associated to the WD disruption. Assuming disruption outside the last stable orbit, part of the WD material will settle in an accretion disk powering a luminous X-ray source that will be detectable up to ~ 200 Mpc. A small fraction of the debris will become unbound forming a thin arc or annulus that expands at nearly the escape velocity. Photoionization of this annulus by X-ray and UV photons produced by the accretion process will result in several different (depending on the WD composition) emission lines, with relative intensities changing on a timescale of a week as the debris expands. Such lines will be observable well beyond 100 Mpc with future 30m-class telescopes and provide a unique signature of this kind of events. If disruptions during the final plunge also result in observable electro-magnetic flares, the detection rate would increase by a factor of ~ 3 (see table 1) considering Schwarzschild MBHs. However whether such a disruption would produce an observable signal is an open question that we have not tried to address here and deserves further investigation.

Based on the above results it is conceivable that several MBH-WD binary systems will be observed both in gravitational wave and electro-magnetic band at a distance up to a few hundreds of Mpc; however no events as well as hundreds of events are consistent with our current understanding of the key physical processes.

The need to observe MBH-WD binaries in the electro-magnetic and gravitational window to maximise the science return raises the issue of *prompt alerts* generated by *LISA* to electro-magnetic observatories. So far alerts have been discussed only in the context of observations of massive-black hole binary systems (*e.g.* Kocsis et al 2006, 2007a,b; Lang & Hughes 2008), but the scenario that we have discussed in this paper calls for a systematic study regarding extreme-mass ratio-inspirals in the relevant mass range. Unfortunately, the complexity of searches for EMRIs and the still limited understanding and maturity of end-to-end algorithms (*e.g.* Babak et al. 2008; Gair et al. 2008a,b; Cornish 2008) prevent at present a realistic study of such an important problem.

ACKNOWLEDGMENTS

Support for this work was provided by NASA through grant GO-10131 from the Space Telescope Science Institute and through grant ATP NNG04GU99G. Partial support was provided by a grant from the NSF, PHY 02-03046. A.S is supported by the CGWP at Penn State University. A.V is supported by the UK Science and Technology Facilities Council. A.V., M.E. and S.S. acknowledge support from the Theoretical Astrophysics Visitors' Fund at Northwestern University and thanks the members of the group for their warm hospitality during their stay. A.S. and S.S. thank the Aspen Center for Physics for hospitality.

REFERENCES

Alexander T., 2007, preprint, arXiv0708.0688
 Aller M. C. & Richstone D., 2002, AJ, 124, 3035

Amaro-Seoane P., Gair J. R., Freitag M., Miller M. C., Mandel I., Cutler C. J. & Babak S., 2007, astro-ph/0703495
 Anders E. & Grevesse N., 1989, Geochimica et Cosmochimica Acta, 53, 197
 Arun, K. G., Iyer, B. R., Sathyaprakash, B. S., Sinha, S., & van den Broeck, C. 2007, PRD, 76, 104016
 Babak S., et al 2008 Class. Quantum Grav. 25 114037
 Barack L. & Cutler C. J., 2004, PhRvD, 69, 082005
 Barth A. J., Greene J. E. & Ho L. C., 2005, ApJ, 619, 151
 Bender, P. L. et al., 1998 *LISA Pre-Phase A Report; Second Edition*, MPQ 233.
 Cornish, N. J. 2008, ArXiv e-prints, 804, arXiv:0804.3323
 Porter, E. K., & Cornish, N. J. 2008, arXiv:0804.0332
 Cutler, C. 1998, PRD, 57, 7089
 Dotti M., Salvaterra R., Sesana A., Colpi M. & Haardt F., 2006, MNRAS, 372, 869
 Ferland G. J., Korista K. T., Verner D. A., Ferguson J. W., Kingdon J. B. & Verner E. M., 1998, PASP, 110, 761
 Freitag M., 2001, CQGra, 18, 4033
 Gair J. et al, 2004 Class.Quant.Grav. 21, S1595
 Gair, J. R., Babak, S., Porter, E. K., & Barack, L. 2008a, ArXiv e-prints, 804, arXiv:0804.3322
 Gair, J. R, Mandel, I., & Wen, L. 2008b, arXiv:0804.1084
 Gonzlez R. E., Lares M., Lambas D. G. & Valotto C., 2006, A&A, 445, 51
 Greene J. E. & Ho L. C., 2004, ApJ, 610, 722
 Hills D. & Bender P. L., 1995, ApJ, 445, 7
 Holz D. E. & Hughes S. A., 2005, ApJ, 629, 15
 Hopman C. & Alexander T., 2006a, ApJ, 645, 133
 Hopman C. & Alexander T., 2006b, ApJ, 645, 1152
 Hughes, S. A. 2002, MNRAS, 331, 805
 Kocsis, B., Frei, Z., Haiman, Z., & Menou, K. 2006, ApJ, 637, 27
 Kocsis, B., Haiman, Z., Menou, K., & Frei, Z. 2007a, PRD, 76, 022003
 Kocsis, B., Haiman, Z., & Menou, K. 2007b, arXiv:0712.1144
 Ivanov P. B., 2002, MNRAS, 336, 373
 Lang R. N., & Hughes S. A., 2006, PRD, 74, 122001
 Lang, R. N., & Hughes, S. A. 2008, ApJ, 677, 1184
 Madej J. Nalezty M. & Althaus L. G., 2004, A&A, 419, 5
 Magorrian J. & Tremaine S., 1999, MNRAS, 304, 447
 Mathews W. G. & Ferland G. J., 1987, ApJ, 323, 456
 Menou K., 2003, CQGra, 20, 37
 Menou K., Haiman Z. & Kocsis B. 2008, preprint, arXiv:0803.3627
 Metcalfe T. S., 2003, ApJ, 587, L43
 Miller M. C., Freitag M., Hamilton D. P. & Lauburg V. M., 2005, ApJ, 117, 120
 Milosavljević, M., & Phinney, E. S. 2005, ApJ, 622, L93
 Nauenberg M., 1972, ApJ, 175, 417
 Nelemans G., Yungelson L. R. & Portegies-Zwart S. F., 2001, A&A, 375, 890
 Peters P C and Mathews J 1963 Phys. Rev. D 131 435
 Peters P C 1964 Phys. Rev. D 136 B1224
 Rantsiou E., Kobayashi S., Laguna P. & Rasio F., 2008, ApJ, in press, arXiv:astro-ph/0703599
 Sabatini S., Davies J., Scaramella R., Smith R., Baes M., Linder S. M., Roberts S. & Testa V., 2003, MNRAS, 341, 981
 Schutz B. F., 1986, Nature, 323, 310
 Shapiro S. L., 2005, ApJ, 620, 59
 Sigurdsson S. & Rees M. J., 1997, MNRAS, 284, 318
 Staniero O., Domínguez I., Imbriani G. & Piersanti L., 2003, ApJ, 583, 878
 Trentham N. & Tully R. B., 2002, MNRAS, 335, 712
 Trias, M., & Sintes, A. M. 2008, PRD, 77, 024030
 Vallisneri M., 2000, PRL, 84, 3519
 Vecchio A., 2004, PhRvD, 70d2001
 Whitcomb S. L., 2008, Class. Quantum Grav. 25 114013

Wilson G., Smail I., Ellis R. S. & Couch W. J., 1997, *MRASE*,
284, 915